Halide vapor phase epitaxy of twin-free α-Ga_2O_3 on sapphire (0001) substrates

Yuichi Oshima*, Encarnación G. Víllora, and Kiyoshi Shimamura

Optical Single Crystals Group, National Institute for Materials Science, 1-1 Namiki, Tsukuba, Ibaraki 305-0044, Japan

E-mail: OSHIMA.Yuichi@nims.go.jp

The halide vapor phase epitaxy of α-Ga_2O_3 is demonstrated for the first time. The films are twin-free, heteroepitaxially grown on sapphire (0001) substrates using gallium chloride and oxygen as precursors. X-ray ω-2θ and pole figure measurements reveal that the film is single-crystalline (0001) α-Ga_2O_3 with no detectable formation of β-Ga_2O_3. The optical bandgap is determined from the transmittance spectrum to be 5.16 eV. The growth rate monotonically increased with the partial pressures of the raw material gases, reaching approximately 150 μm/h, which is over two orders of magnitude larger than those of conventional vapor phase epitaxial growth techniques, such as mist-CVD or MBE.

Ga_2O_3 is known to possess five different crystal structures, *i.e.*, α-, β-, δ-, ε-, and γ-phase. Among them, β-Ga_2O_3 is thermodynamically the most stable. [1] The bandgap of β-Ga_2O_3 is reported to be 4.7 eV, [2] therefore it is very transparent even in the UV region. In addition, the electrical conductivity can be controlled by the doping with Si or Sn. [3, 4] Furthermore, single crystal substrates produced from melt are available, [5-7] and high-quality homoepitaxial layer can be grown on those substrates. [8-11] Accordingly, β-Ga_2O_3 is attracting remarkable attention as a promising wide bandgap semiconductor for various applications such as substrates for GaN-based LEDs, [12, 13] UV detectors [14], and power devices such as SBDs, [10] MESFETs, [15] and MOSFETs. [16]

On the other hand, α-Ga_2O_3, which is the target material of this work, is a meta-stable phase, and the number of publications is limited compared to those of β-Ga_2O_3. However, α-Ga_2O_3 has also been reported to have a large bandgap energy (E_g = 5.3 eV), [17] and its electrical conductivity can be controlled as well. [18, 19] Furthermore, this compound has been proposed to realize novel functional materials through the formation of solid-solutions with other corundum-structured oxides, such as α-Al_2O_3. [20] α-Ga_2O_3 is thus a very promising wide bandgap semiconductor.

Unfortunately, single crystal substrates of α-Ga_2O_3 cannot be produced from melt, since the material is meta-stable. Accordingly, single crystalline α-Ga_2O_3 films need to be produced by heteroepitaxy. Sapphire is one of the most promising substrate materials, because it possesses the same corundum structure, and large-area high-quality substrates are available at a reasonable price. The lattice mismatches between α-Ga_2O_3 and sapphire along *a*- and *c*-axis are ~4.5% and ~3.3%, respectively.

So far, the vapor phase growth of α-Ga_2O_3 has been demonstrated only by mist-CVD[17-20] and MBE [21]. Kumaran *et al*. reported the MBE of single crystalline Nd-doped α-Ga_2O_3 on sapphire ($11\bar{2}0$) [21]. The α-Ga_2O_3 films grown by mist-CVD on sapphire (0001) exhibited a narrow FWHM (~60 arcsec) of the X-ray rocking curve (XRC) in out-of-plane diffraction, while no data is reported about the in-plane mosaicity. [17-20] The domain-matching epitaxy mechanism has been proposed as the reason for the narrow tilt angle.[22] However, in-plane twinning, with a small fraction of 180° rotational domains, was observed. [17] The maximum reported growth rate is approximately 1 μm/h. [18] High concentrations of impurities have

been reported for nominally un-doped films ([H] = 3×10^{19} cm^{-3}, [C] = 1×10^{19} cm^{-3}, [Si] = 9×10^{18} cm^{-3}). [19)]

In this work, we have employed the halide vapor phase epitaxy (HVPE) [23)] to grow α-Ga_2O_3 layers. HVPE is a kind of CVD technique, which is characterized by a large growth rate and a high-purity of the resulting crystals. HVPE is nowadays widely used in III-V semiconductors industry. [24)] Regarding the HVPE of Ga_2O_3, there are some publications about β-Ga_2O_3. [11, 25-27)] However, there is no report about the HVPE of α-Ga_2O_3. In this work, we demonstrate the successful high-speed growth of high-purity α-Ga_2O_3 layers by HVPE.

The HVPE growth was conducted in an atmospheric horizontal reactor using gallium chloride and O_2 (> 99.99995% pure) as the precursors. The gallium chloride was synthesized through the chemical reaction between Ga metal (> 99.99999% pure) and HCl gas (> 99.999% pure) upstream in the reactor. The partial pressures of the HCl and O_2 (P(HCl) and P(O_2)) were 0.1 - 0.75 kPa and 0.5 - 6 kPa, respectively. N_2 (> 99.9999% pure) was used as the carrier gas. The deposition temperature was fixed within the range 525-650°C. We used sapphire (0001) substrates.

The surface morphology of the films was observed by scanning electron microscopy (SEM). The growth rate was determined by cross-sectional SEM. The crystal structure and orientation were investigated by X-ray diffraction (XRD) ω-2θ scan and pole figure measurements. The structural quality was estimated by XRC measurement. The impurities concentrations were evaluated by secondary ion mass spectrometry (SIMS). Optical transmittance spectrum was utilized to determine the optical bandgap. The baseline was measured with a sapphire blank substrate.

Firstly, we investigated the influence of the growth temperature under the fixed partial pressures of P(HCl) = 0.25 kPa and P(O_2) = 1.0 kPa. The whole area of each film grown below 575°C was specular for human eyes. SEM images of a film grown at 550°C are shown in Fig.1. However, some random surface areas of the films grown at 575°C or higher temperatures exhibited a rough morphology, which appears mat white for human eyes. The area of such translucent regions increased with the temperature. X-ray ω-2θ scan profiles (not shown) revealed that poly-crystalline β-Ga_2O_3 is dominant in such areas, while the other mirror-like areas were confirmed to be single crystalline α-Ga_2O_3 through

pole figure measurement. The mirror-like area completely disappeared at 650°C. The temperature at which pure α-Ga_2O_3 is obtained is different depending on the report. Shinohara and Fujita reported that α-Ga_2O_3 was dominant under 630°C, and no β-Ga_2O_3 was detected below 470°C [17] in the Ga_2O_3 film grown by mist-CVD. In contrast, β-Ga_2O_3 was still dominant at 500°C in MBE-grown Ga_2O_3 films on *c*-plane sapphire. [21, 29] Such differences could be originated not only on the accuracy of the growth temperature, but also on the intrinsic nature of each growth method, therefore a detailed explanation is difficult at present. Because our HVPE and the mist-CVD both include H_2O and HCl in the atmosphere, we speculate that such molecules could play a key role.

The temperature dependence of the growth rate at the mirror-like area is presented in Fig.2. The growth rate exhibited a significant increase with the temperature rise. This could be explained by the change of the molar ratio of GaCl and $GaCl_3$ generated in the Ga container. Figure 3 shows the calculated partial pressures of GaCl and $GaCl_3$ in the equilibria Ga + HCl = GaCl + 1/2H_2 and GaCl + 2HCl = $GaCl_3$ + H_2, respectively. The detailed procedure of the thermodynamic analysis has been described elsewhere. [28] The calculation was carried out assuming the injection of the HCl gas into the Ga container with a partial pressure of 5 kPa and using N_2 as the carrier gas, in accordance with the actual experimental condition. Note that the Ga temperature should be close to the growth temperature, since the Ga container and the substrate holder were nearby in a single zone hot-wall furnace. It can be seen that the mole fraction of $GaCl_3$ continuously decreases with increasing temperature, being negligible above 600°C. On the contrary, GaCl rises significantly with the temperature from 250 to 500°C, where it starts to saturate towards 600°C. Taking both into account, at the considered deposition temperatures the decrease of $GaCl_3$ is largely compensated by the increase in GaCl. As a result, this enhancement of Ga transport can be responsible for the increase in deposition rate.

Secondly, we describe the characterization of the α-Ga_2O_3 films (3.6 μm thick) grown at 550°C under the partial pressures of P(HCl) = 0.25 kPa and P(O_2) = 1.0 kPa. The XRD ω-2θ scan profile of the film is shown in Fig.4(a) and (b). Apart from the peaks of the sapphire substrate, only the allowed reflections from the *c*-plane of α-Ga_2O_3 were observed. Therefore, the film is composed of only the (0001)-oriented α-Ga_2O_3 phase, with no detectable admixture of the β-Ga_2O_3 phase.

Figures 5(a) and (b) are the $\{10\bar{1}2\}$ pole figures of the film and the sapphire substrate, respectively. Three peaks appeared at the positions which are expected for single crystalline α-Ga_2O_3, indicating that the film is single crystalline. This result contrasts with the reported in Ref.17, where three additional reflections were observed with a rotation angle of 180° relative to the former ones. Therefore, our diffraction measurements prove that twin-free α-Ga_2O_3 was deposited heteroepitaxially on sapphire (0001) for the first time. The epitaxial relationships are elucidated as:

$[10\bar{1}0]$ α-Ga_2O_3 // $[10\bar{1}0]$ sapphire and (0001) α-Ga_2O_3 // (0001) sapphire

Figure 6 shows the XRC profiles of (0006) and $(10\bar{1}2)$ diffraction peaks measured in symmetric and skew-symmetric geometry, respectively. The FWHM of the (0006) diffraction, with 612 arcsec, reflects the tilting of the *c*-plane. The FWHM of $(10\bar{1}2)$ diffraction (whose plane is 57.6^{o} inclined from the *c*-plane) in skew-symmetry, with 1296 arcsec, indicates the twisting around the *c*-axis. Smaller values of FWHM are notably favored by a slower growth rate during nucleation. Therefore, the structural quality of the HVPE epilayers can be remarkably improved by optimizing the growth conditions at the initial growth stage.

The results of the SIMS measurement is given in Table I. [H], [C] were below the detection limit, in contrast to the high values [H] = 3×10^{19} cm^{-3} and [C] = 1×10^{19} cm^{-3} reported in Ref.19. This is probably due to the fact that HVPE does not use organic compounds as raw materials. [Al] was also below the detection limit. In addition, [Si] was also much lower than the reported value. [19] Although [Cl] cannot be compared because there is no past report, it might be worth to mention that a value as low as [Cl] = 1×10^{16} cm^{-3} was determined for a homoepitaxial β-Ga_2O_3 layer grown by HVPE at 1000°C. [26] A plausible explanation for the difference in [Cl] is that the desorption of chlorine atoms from the growth front is favored through the temperature rise.

Figure 7 shows the transmittance *T*. Although the optical transition type of α-Ga_2O_3 is still under discussion, we estimated the bandgap energy to be 5.16 eV through the $(h\nu\alpha)^2$ - $(h\nu)$ plot (inset of Fig.7).

Finally, we tried further high-speed growth. The growth rate of α-Ga_2O_3 at 550°C as a

function of the partial pressures of $P(O_2)$ and P(HCl) is shown in Figs.8(a) and (b), respectively. The growth rate monotonically increased with increasing the partial pressures, showing a saturating tendency at high partial pressures. The growth rate reaches approximately 150 μm/h, which is over two orders of magnitude greater than those of other epitaxial techniques, such as mist-CVD or MBE. The surface was still mirror-like, and the pole figure was confirmed to be that of single crystal even at the largest growth rate. The saturation in Fig.8(a) is probably due to the shortage of gallium chloride. Actually, the further increase of the growth rate at $P(O_2)$ = 4.0 kPa by increasing the P(HCl) is confirmed in Fig.8(b). On the other hand, the saturation tendency in Fig.8(b) is likely to be caused by the limitation of the chemical reactions at the considered temperatures to generate gallium chloride and/or Ga_2O_3. Insufficient mixing of gallium chloride and O_2 could also contribute to the saturation.

In summary, present work demonstrates for the first time the successful heteroepitaxial growth of twin-free α-Ga_2O_3 on *c*-plane sapphire substrates by HVPE. The epitaxial relationships were determined to be [$10\bar{1}0$] α-Ga_2O_3 // [$10\bar{1}0$] sapphire and (0001) α-Ga_2O_3 // (0001) sapphire, in good accordance with the corundum structure of both compounds. Impurity concentrations ([H], [C], and [Si]) were much lower than the reported values by factors in the range of 100-1000. The optical bandgap was estimated to be 5.16 eV. The growth by HVPE reached a maximum rate of approximately 150 μm/h, which is over two orders of magnitude greater than the reported so far. Present results confirm the high potential of the HVPE for the growth of thick films or even free-standing α-Ga_2O_3 wafers.

Acknowledgment

This work was partly supported by a Grant-in-Aid for Scientific Research (C) No. 25420307 from Japan Society for the Promotion of Science (JSPS).

References

1) R. Roy, V. G. Hill, and E. F. Osborn, J. Am. Chem. Soc. **74**, 719 (1952).

2) H. H. Tippins, Phys. Rev. **140**, A316 (1965).

3) N. Suzuki, S. Ohira, M. Tanaka, T. Sugawara, K. Nakajima, and T. Shishido: Phys. Status. Solidi C **4**, 2310 (2007).

4) E. G. Víllora, K. Shimamura, Y. Yoshikawa, T. Ujiie, and K. Aoki: Appl. Phys. Lett **92**, 202120 (2008).

5) E.G. Víllora, K. Shimamura, Y. Yoshikawa, K. Aoki, N. Ichinose, J. Cryst. Growth **270**, 420 (2004).

6) H. Aida, K. Nishiguchi, H. Takeda, N. Aota, K. Sunakawa, Y. Yaguchi, Jpn. J. Appl. Phys. **47**, 8506 (2008).

7) Z. Galazka, K. Irmscher, R. Uecker, R. Bertram, M. Pietsch, A. Kwasniewski, M. Naumann, T. Schulz, R. Schewski, D. Klimm, and M. Bickermann, J. Cryst. Growth **404**, 184 (2014).

8) E.G. Víllora, K. Shimamura, K. Kitamura, and K. Aoki, Appl. Phys. Lett. **88**, 031105 (2006).

9) T. Oshima, N. Arai, N. Suzuki, S. Ohira, and S. Fujita, Thin Solid Films **516**, 5768 (2008).

10) K. Sasaki, A. Kuramata, T. Masui, E.G. Víllora, K. Shimamura, and S. Yamakoshi, Appl. Phys. Express **5**, 035502 (2012).

11) K. Nomura, K.Goto, R.Togashi, H. Murakami, Y. Kumagai, A. Kuramata, S. Yamakoshi, A. Koukitu, J. Cryst. Growth **405**, 19 (2014).

12) K. Shimamura, E.G. Víllora, K. Domen, K. Yui, K. Aoki, N. Ichinose, Jpn. J. Appl. Phys. **44**, L7 (2005).

13) E.G. Víllora, S. Arjoca, K. Shimamura, D. Inomata, K. Aoki, Proc. SPIE 8987, Oxide-based Materials and Devices V, 89871U, March 8 (2014).

14) T. Oshima, T. Okuno, N. Arai, N. Suzuki, S. Ohira, and S. Fujita, Appl. Phys. Express **1**, 011202 (2008).

15) M. Higashiwaki, K. Sasaki, A. Kuramata, T. Masui, S. Yamakoshi, Appl. Phys. Lett. **100**, 013504 (2012).

16) M. Higashiwaki, K. Sasaki, T. Kamimura, M.H. Wong, D. Krishnamurthy, A. Kuramata, T. Masui, S. Yamakoshi, Appl. Phys. Lett. **103**, 123511 (2013).

17) D. Shinohara and S. Fujita, Jpn. J. Appl. Phys. **47**, 7311 (2008).

18) T. Kawaharamura, G. T. Dang, and M. Furuta, Jpn. J. Appl. Phys. **51**, 040207 (2012).

19) K. Akaiwa and S. Fujita, Jpn. J. Appl. Phys. **51**, 070203 (2012).

20) S. Fujita and K. Kaneko, J. Cryst. Growth **401**, 588 (2014).

21) R. Kumaran, T. Tiedje, S.E. Webster, S. Penson, and W. Li, Opt. Lett. **35**, 3793 (2010).

22) K. Kaneko, H. Kawanowa, H. Ito, and S. Fujita, Jpn. J. Appl. Phys. **51**, 020201 (2012).

23) J. J. Tietjen and J. A. Amic, J. Electrochem. Soc. **113**, 724 (1966).

24) Y. Oshima, T. Eri, M. Shibata, H. Sunakawa, K. Kobayashi, T. Ichihashi, and A. Usui, Jpn. J. Appl. Phys. **42**, L1 (2003).

25) T. Matsumoto, M. Aoki, A. Kinoshita, T. Aono, Jpn. J. Appl. Phys. **13**, 1578 (1974).

26) H. Murakami, K. Nomura, K. Goto, K. Sasaki, K. Kawara, Q. T. Thieu, R. Togashi, Y. Kumagai, M. Higashiwaki, A. Kuramata, S. Yamakoshi, B. Monemar and A. Koukitu, Appl. Phys. Express **8**, 015503 (2015).

27) Y. Oshima. E. G. Víllora, and K. Shimamura, J. Cryst. Growth **410**, 53 (2015).

28) V. S. Ban, M. Ettenberg, J. Phys. Chem. Solids **34**, 1119 (1973).

29) T. Oshima, T. Okuno, and S. Fujita, Jpn. J. Appl. Phys. **46**, 7217 (2007).

Figure Captions

Fig. 1. SEM images of an α-Ga_2O_3 layer grown on a sapphire (0001) substrate. (a) surface image, (b) cross-sectional image.

Fig. 2. Growth rate of α-Ga_2O_3 as a function of growth temperature.

Fig. 3. Calculated partial pressures of GaCl and $GaCl_3$ in equilibrium as a function of temperature (result of thermodynamic analysis).

Fig. 4. XRD ω-2θ profile of an α-Ga_2O_3 layer grown on a sapphire (0001) substrate. (a) wide-scan profile, (b) narrow-scan profile around (0006).

Fig. 5. X-ray $\{10\bar{1}2\}$ pole figures (log-scale) of (a) α-Ga_2O_3 layer and (b) sapphire substrate.

Fig. 6. XRCs of an α-Ga_2O_3 film.

Fig. 7. Transmittance spectra of α-Ga_2O_3. The inset shows the absorption coefficient in $(h\nu\alpha)^2$ vs $h\nu$.

Fig. 8. Growth rate of α-Ga_2O_3 as a function of (a) O_2 partial pressure, (b) HCl partial pressure.

Table I. Impurity concentrations in α-Ga_2O_3 measured by SIMS.

Element	Detection limit (D. L.) [cm^{-3}]	Concentration [cm^{-3}]
H	4×10^{17}	< D. L.
C	6×10^{17}	< D. L.
Al	4×10^{15}	< D. L.
Si	1×10^{16}	2×10^{16}
Cl	1×10^{16}	7×10^{16}

Figures

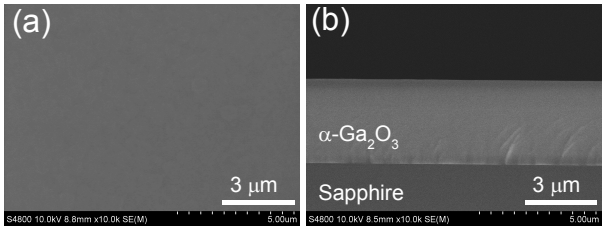

Fig. 1

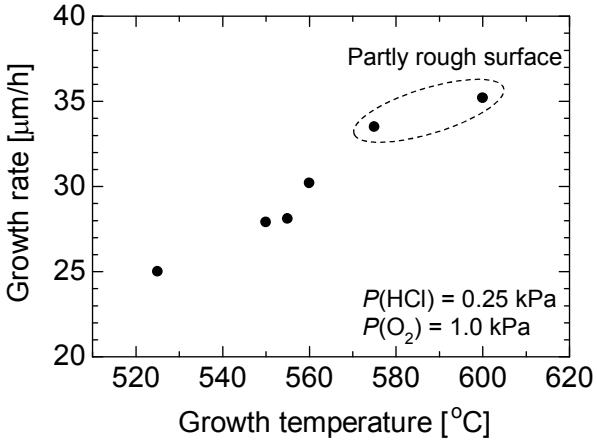
Partly rough surface
P(HCl) = 0.25 kPa
P(O2) = 1.0 kPa
Growth rate [μm/h]
Growth temperature [°C]
40
35
30
25
20
520
540
560
580
600
620

Fig. 2

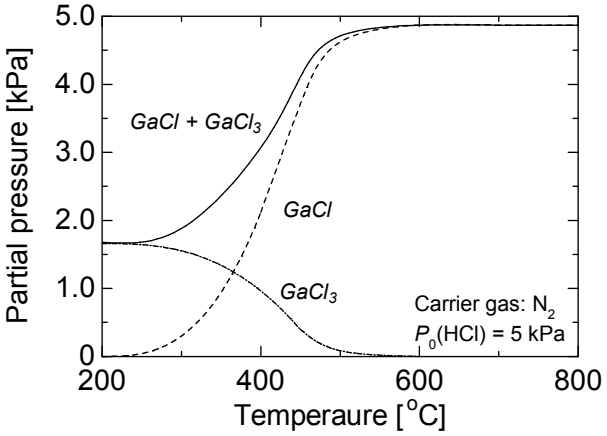
5.0
4.0
3.0
2.0
1.0
0
Partial pressure [kPa]
GaCl + GaCl3
GaCl
GaCl3
Carrier gas: N2
P0(HCl) = 5 kPa
200
400
600
800
Temperaure [°C]

Fig. 3

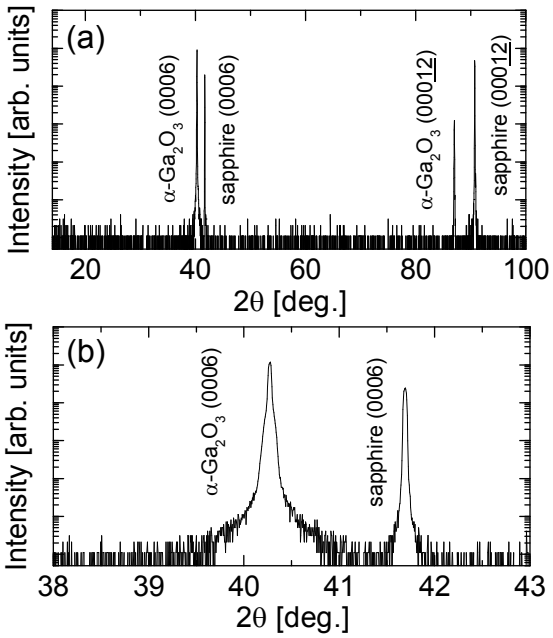
(a)
Intensity [arb. units]
α-Ga2O3 (0006)
sapphire (0006)
α-Ga2O3 (0001̄2)
sapphire (0001̄2)
20
40
60
80
100
2θ [deg.]
(b)
Intensity [arb. units]
α-Ga2O3 (0006)
sapphire (0006)
38
39
40
41
42
43
2θ [deg.]

Fig. 4

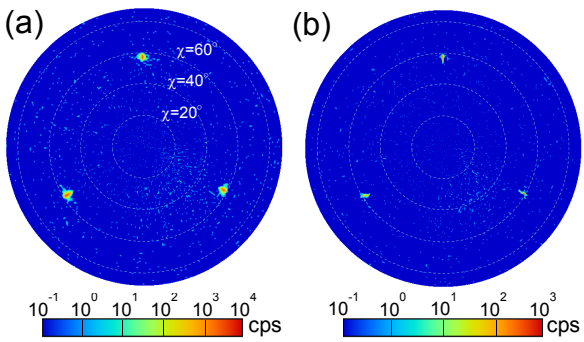
(a)
χ=60°
χ=40°
χ=20°
10^-1 10^0 10^1 10^2 10^3 10^4
cps
(b)
10^-1 10^0 10^1 10^2 10^3
cps

Fig. 5

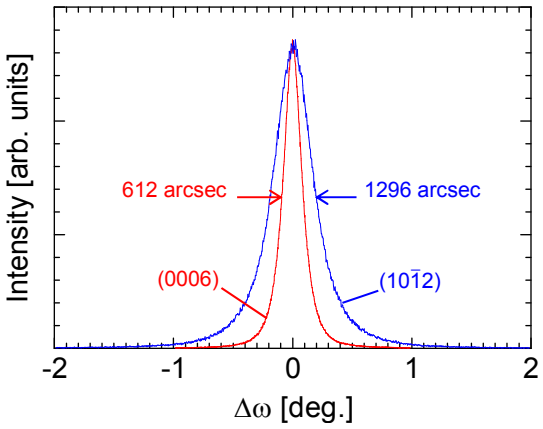
Intensity [arb. units]
612 arcsec
1296 arcsec
(0006)
(10$\bar{1}$2)
-2
-1
0
1
2
Δω [deg.]

Fig. 6

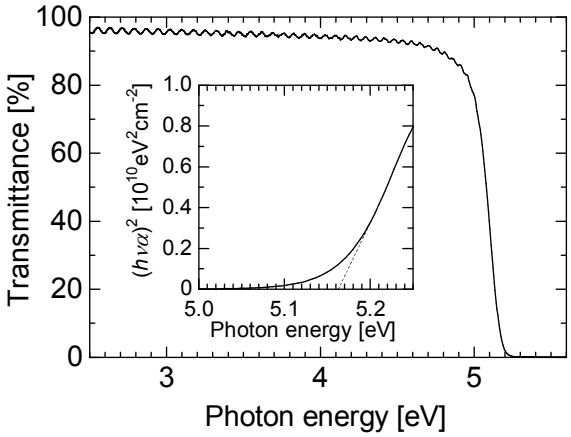
Transmittance [%]
Photon energy [eV]
$(h\nu\alpha)^2$ [10^{10}eV^{2}cm^{-2}]
Photon energy [eV]

Fig. 7

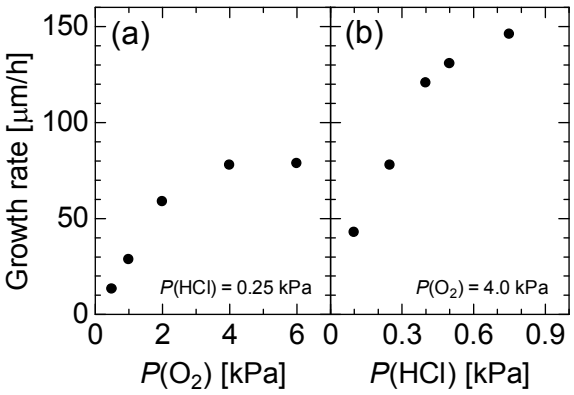
(a)
(b)
Growth rate [μm/h]
150
100
50
0
0
2
4
6
0
0.3
0.6
0.9
P(HCl) = 0.25 kPa
P(O2) = 4.0 kPa
P(O2) [kPa]
P(HCl) [kPa]

Fig. 8